remote sensing

MDPI

Article

On the Choice of the Third-Frequency Galileo Signals in Accelerating PPP Ambiguity Resolution in Case of Receiver Antenna Phase Center Errors

Shaoming Xin [1], Jianghui Geng [1,*], Jiang Guo [1] and Xiaolin Meng [2]

[1] GNSS Research Center, Wuhan University, Wuhan 430079, China; sxin@whu.edu.cn (S.X.); guojiang@whu.edu.cn (J.G.)

[2] Nottingham Geospatial Institute, University of Nottingham, Nottingham NG7 2RD, UK; xiaolin.meng@nottingham.ac.uk

* Correspondence: jgeng@whu.edu.cn; Tel.: +86-027-68778955

Received: 9 February 2020; Accepted: 17 April 2020; Published: 22 April 2020

Abstract: Rapid precise point positioning ambiguity resolution (PPP-AR) is of great importance to improving precise positioning efficiency. There is an expectation that Galileo multi-frequency (three or more frequencies) data processing will offer a promising way to accelerate PPP-AR. However, the performance of different combination observables out of raw Galileo multi-frequency data is still unclear, and the adverse impacts of missing receiver antenna phase center corrections have not been quantified in detail. We therefore studied uncombined Galileo PPP-AR by contrasting three typical triple-frequency combinations, which are E1/E5a/E5b, E1/E5a/E6, and E1/E5/E6 signals, using 30 days of data from 15 stations across Australia. We carried out triple-frequency PPP-AR by separately applying the official GPS receiver antenna phase centers, as currently employed in most relevant literatures, as well as the pilot Galileo receiver antenna phase centers preliminarily measured by the International GNSS Service. We found that, compared to dual-frequency (E1/E5a) PPP-AR, triple-frequency PPP-AR based on E1/E5a/E5b signals shortened the convergence time by only 7.6%, while those based on E1/E5a/E6 and E1/E5/E6 increased unexpectedly the convergence time by 17.6% and 12.7%, respectively, if the GPS receiver antenna corrections were presumed for Galileo signals. However, after using the pilot Galileo phase center corrections, triple-frequency PPP-AR based on E1/E5a/E5b, E1/E5a/E6, and E1/E5/E6 signals could speed up the convergence on average by about 16.2%, 30.3%, and 17.7%, respectively. Therefore, we demonstrate the critical impact of correct Galileo receiver antenna phase centers on multi-frequency PPP-AR convergences. Moreover, the triple-frequency signal combination E1/E5a/E6 is advantageous over others in achieving rapid triple-frequency Galileo PPP-AR.

Keywords: Galileo; triple-frequency; precise point positioning; ambiguity resolution; rapid convergence; phase center errors

1. Introduction

Precise point positioning (PPP) can provide centimeter-level positioning without reference stations in contrast to real-time kinematic (RTK) positioning, which can achieve centimeter-level positioning based on short baselines of a few kilometers to a reference station [1,2]. Although RTK requires a dense network of reference stations, it can resolve the ambiguity instantaneously or in a few minutes while PPP cannot. Therefore, the main limitation of PPP is the slow convergence, which usually takes tens of minutes of continuous phase observations [3].

With the development of PPP, an increasing number of strategies are emerging to speed up the convergence or ambiguity resolution (PPP-AR). Data processing based on dual-frequency multi-GNSS

observations from GPS, GLONASS, and BeiDou with a regional network of GNSS reference stations can obtain ambiguity-fixed solutions within only 10 min [4]. Multi-GNSS can make more satellites available and thus improve the strength of satellite geometry [5]. However, dual-frequency GPS-only solutions generally need over 30 min to resolve ambiguities properly. Using precise atmosphere corrections is a feasible way to shorten this convergence time, but it has a drawback of requiring a dense reference network [6,7]. Thanks to the enhanced satellite geometry and the improved partial ambiguity fixing strategy, Geng and Shi (2017) accomplished GPS and GLONASS PPP-AR within about 6 min by resolving undifferenced GPS and GLONASS ambiguities simultaneously [8].

Besides multi-GNSS observations and precise atmosphere corrections, the use of multi-frequency GNSS observations is also helpful. A typical and representative example is Galileo, which transmits E1/E5a/E5b/E5/E6 signals. Multi-frequency Galileo signals can form various carrier-phase combinations of longer wavelengths, thereby contributing to fast ambiguity resolution and improving positioning precision during the convergence period [9–11].

Li et al. (2018) carried out BeiDou triple-frequency PPP-AR in a large network covering Southeast Asia and Australia [12]. Their results indicate it is possible to reduce the average convergence time from 34 to 28 min by integrating the third frequency B3I. Geng and Bock (2013) used GPS L1, L2, and L5 signals to form an ionosphere-free wide-lane combination, which can be further used to accelerate narrow-lane ambiguity resolution [13]. They found that the wide-lane ambiguity could still be resolved efficiently even when the noise of the combination was amplified by over 100 times; as a result, 78% of the PPP-AR solutions could be accomplished within 2 min. Geng et al. (2020) used triple-frequency GPS/BeiDou/Galileo/QZSS data and achieved triple-frequency PPP-AR in 6 min on average. However, (extra-)wide-lane ambiguity resolution, though expected to assist in speeding up narrow-lane ambiguity resolution, might sometimes deteriorate PPP convergences compared to dual-frequency PPP-AR [14]. Cao et al. (2018) used an uncombined PPP model to study triple-frequency PPP-AR using Galileo E1/E5a/E5b signals; their results also indicated that some ambiguities were not fixed successfully to integers which might be imputed to unmodeled errors such as antenna phase centers; note that the International GNSS Service (IGS) has not released official phase center corrections for Galileo stations [15]. Hence, while the third frequency of GNSS signals has been demonstrated to have the potential to shorten the convergence time of PPP-AR, it is still interesting to investigate how each of the candidate third-frequency signals contributes to fast PPP-AR. Moreover, the impact of receiver antenna phase center errors on triple-frequency Galileo PPP-AR is also worthy of investigation.

In this study, we mainly analyze how the choice of triple-frequency signals improves PPP-AR or convergence in the case of Galileo multi-frequency data. The impact of receiver antenna phase center errors will also be investigated. This paper first introduces the method of undifferenced uncombined triple-frequency PPP-AR in Section 2. The required data and the processing strategies are introduced in Section 3. In Section 4, we present the results, including the characteristics of the Galileo signals on different frequencies, evaluation of estimated Galileo phase biases and the performances of the Galileo triple-frequency PPP-AR with and without the use of pilot Galileo receiver antenna phase center offsets and variations (PCO/PCV) corrections. Furthermore, we discuss the choice of triple-frequency signals and the effects of receiver antenna phase center errors in Section 5. The final section provides the conclusions of the study.

2. Methods

2.1. Undifferenced Uncombined Triple-Frequency Observation Equations

Considering the pseudo-range and carrier-phase hardware biases of satellites and receivers, the raw Galileo observation equations between station i and satellite j for three frequencies ($n = 1, 2, 3$) are written as:

$$\begin{cases} P_{i.n}^{j} = \rho_i^j + c(t_i - t^j) + m_i^j T_i + I_{i,n}^j + B_{i,n} - B_n^j \\ L_{i,n}^{j} = \rho_i^j + c(t_i - t^j) + m_i^j T_i - I_{i,n}^j + \lambda_n (N_{i,n}^j + b_{i,n} - b_n^j) \end{cases} \quad (1)$$

where $P_{i,n}^{j}$ and $L_{i,n}^{j}$ are the pseudo-range and carrier-phase observations on three frequencies of Galileo satellites, respectively, which can be any three of the E1/E5a/E5/E5b/E6 signals. ρ_i^j is the geometric distance between the station and the satellite. c is the speed of light in vacuum. t_i and t^j are the receiver and satellite clock errors, respectively. m_i^j is the mapping function, and T_i is the zenith tropospheric wet delay of the corresponding station. $I_{i,n}^{j}$ is the first-order ionosphere delay, and $I_{i,2}^{j} = g_2^2 I_{i,1}^{j}$ and $I_{i,3}^{j} = g_3^2 I_{i,1}^{j}$. g_2 and g_3 represent the corresponding scaling coefficients which equate $\frac{f_1}{f_2}$ and $\frac{f_1}{f_3}$, respectively (f_1, f_2, and f_3 are the selected frequencies of Galileo signals). $B_{i,n}$ and B_n^j are the pseudo-range hardware biases at the station and satellite ends, respectively. λ_n is the corresponding wavelength. $b_{i,n}$ and b_n^j are the phase biases at the station and satellite ends, respectively. $N_{i,n}^{j}$ is the integer ambiguity.

Nevertheless, it is not possible to solve the above raw equations directly due to rank deficiency caused by the linear dependency among hardware biases, ambiguities, and clock error parameters. Therefore, it is necessary to implement re-parameterize strategies where hardware biases are incorporated into the clock error and ionosphere delay parameters [16,17]. The ambiguity terms also absorb some biases during the parameterization. In this study, the uncombined triple-frequency PPP model takes the form as Equation (2),

$$\begin{cases} P_{i,n}^{j} = \rho_i^j + c(\hat{t}_i - \hat{t}^j) + m_i^j T_i + \hat{I}_{i,n}^{j}; & (n = 1,2) \\ P_{i,n}^{j} = \rho_i^j + c(\hat{t}_i - \hat{t}^j) + m_i^j T_i + \hat{I}_{i,n}^{j} + h_i^j; & (n = 3) \\ L_{i,n}^{j} = \rho_i^j + c(\hat{t}_i - \hat{t}^j) + m_i^j T_i - \hat{I}_{i,n}^{j} + \lambda_n \hat{N}_{i,n}^{j}; & (n = 1,2,3) \end{cases} \tag{2}$$

Equations (3)–(6) clearly show the formulation of each re-parameterized unknown from Equation (2). In detail, Equation (3) shows the common parameters for all triple-frequency equations. $\hat{t}_i$ is the new time-varying receiver clock error parameter which contains the pseudo-range hardware biases of the receiver. $\hat{t}^j$ is the new time-varying satellite clock error parameter which is estimated based on the ionosphere-free L1/L2 combination.

$$\begin{cases} \hat{t}_i = t_i + \frac{(g_2^2 B_{i,1} - B_{i,2})}{c(g_2^2 - 1)} \\ \hat{t}^j = t^j + \frac{(g_2^2 B_1^j - B_2^j)}{c(g_2^2 - 1)} \end{cases} \tag{3}$$

Equation (4) shows an additional parameter h_i^j estimated within the third-frequency pseudo-range equation. It is a station-satellite-specific and time-constant parameter for extracting the inter-frequency bias between the L1/L2 and L3 pseudo-range [18]. α and β are ionosphere-free combination coefficients computed by g_2, where $\alpha = \frac{g_2^2}{g_2^2 - 1}$ and $\beta = \frac{1}{g_2^2 - 1}$.

$$h_i^j = g_3^2 \beta (B_{i,1} - B_{i,2}) - (\alpha B_{i,1} - \beta B_{i,2}) + B_{i,3} - g_3^2 \beta (B_1^j - B_2^j) + \alpha B_1^j - \beta B_2^j - B_3^j \tag{4}$$

Equations (5) and (6) show the other parameters for the equations with different frequencies. $\hat{I}_{i,n}^{j}$ is the new ionosphere delay parameter which has absorbed the pseudo-range hardware biases.

$$\begin{cases} \hat{I}_{i,n}^{j} = I_{i,n}^{j} - \beta (B_{i,1} - B_{i,2} - B_1^j + B_2^j); & (n = 1) \\ \hat{I}_{i,n}^{j} = I_{i,n}^{j} - g_n^2 \beta (B_{i,1} - B_{i,2} - B_1^j + B_2^j); & (n = 2,3) \end{cases} \tag{5}$$

$\hat{N}_{i,n}^{j}$ is the re-parameterized ambiguity parameter which has absorbed phase and pseudo-range biases from the receiver and satellite.

$$\begin{cases} \hat{N}_{i,1}^{j} = N_{i,1}^{j} + b_{i,1} - b_{1}^{j} - \frac{((\alpha+\beta)B_{i,1} - 2\beta B_{i,2} - (\alpha+\beta)B_{1}^{j} + 2\beta B_{2}^{j})}{\lambda_1} \\ \hat{N}_{i,2}^{j} = N_{i,2}^{j} + b_{i,2} - b_{2}^{j} - \frac{(2\beta B_{i,1} - (\alpha+\beta)B_{i,2} - 2\beta B_{1}^{j} + (\alpha+\beta)B_{2}^{j})}{\lambda_2} \\ \hat{N}_{i,3}^{j} = N_{i,3}^{j} + b_{i,3} - b_{3}^{j} - \frac{(g_3^2\beta(B_{i,1} - B_{i,2}) + \alpha B_{i,1} - \beta B_{i,2} - g_3^2\beta(B_{1}^{j} - B_{2}^{j}) - \alpha B_{1}^{j} + \beta B_{2}^{j})}{\lambda_3} \end{cases} \tag{6}$$

In the satellite clock estimation, station coordinates are fixed with daily static PPP solutions while $\hat{t}_i$, $\hat{t}^j$, h_i^j, $\hat{N}_{i,n}^{j}$, and T_i parameters are estimated as usual. Note that a zero-mean constraint was added on all receiver clock parameters to overcome the linear-dependency between receiver and satellite clocks. In PPP, the station coordinates should be estimated by fixing parameter $\hat{t}^j$. In addition, we did not take the higher-order ionosphere delays and the multipath effect into account.

2.2. Estimation of Satellite Phase Biases

The satellite phase fractional-cycle biases are the fractional parts of uncalibrated phase delays originating in the satellite hardware biases (henceforward termed satellite phase biases) [19], which are generally estimated based on a reference network. The phase biases can contaminate the integer carrier-phase ambiguities and destroy the integer nature of ambiguities. Therefore, it is necessary to correct the phase biases first before the ambiguity resolution.

In this study, we estimated the extra-wide-lane, wide-lane, and narrow-lane phase biases and resolved the combined ambiguities correspondingly. Firstly, L1/L2/L3 float ambiguities were estimated according to Equation (2) by fixing the stations' coordinates and satellite clock; then the undifferenced (extra-)wide-lane and ionosphere-free ambiguities ($\hat{N}_{i,ew}^{j}$, $\hat{N}_{i,w}^{j}$, $\hat{N}_{i,if}^{j}$) could be computed according to Equation (7) and the first equation of (9). Note the hat "$\wedge$" denotes an estimated float value and "$\cup$" denotes the corresponding integer part. To eliminate the effect of hardware delays of the receiver end, the single-difference ambiguities between satellite j and satellite k for the station i are formed. As a result, we got single-difference extra-wide-lane and wide-lane float ambiguities $\hat{N}_{i,ew}^{jk}$ and $\hat{N}_{i,w}^{jk}$, which were contaminated by the satellite-pair phase biases only. Next, the satellite-pair extra-wide-lane and wide-lane phase biases ($\hat{b}_{ew}^{jk}$ and $\hat{b}_{w}^{jk}$) can be computed through rounding operations as shown in Equation (8). The operation is defined as $\langle\Theta\rangle = [\Theta] - \Theta$ and $[\Theta]$ is the integer rounding operation.

$$\begin{cases} \hat{N}_{i,ew}^{j} = \hat{N}_{i,2}^{j} - \hat{N}_{i,3}^{j} \\ \hat{N}_{i,w}^{j} = \hat{N}_{i,1}^{j} - \hat{N}_{i,2}^{j} \end{cases} \tag{7}$$

$$\begin{cases} \hat{b}_{ew}^{jk} = \left\langle \hat{N}_{i,ew}^{jk} \right\rangle \\ \hat{b}_{w}^{jk} = \left\langle \hat{N}_{i,w}^{jk} \right\rangle \end{cases} \tag{8}$$

Similarly, we can obtain the single-difference narrow-lane float ambiguity $\hat{N}_{i,1}^{jk}$ and the narrow-lane phase bias $\hat{b}_{n}^{jk}$ by resolving Equations (9)–(11), respectively. It is noted that the integer wide-lane ambiguity should have been recovered before forming narrow-lane ambiguity. The narrow-lane ambiguity has the same value as the L1 ambiguity.

$$\hat{N}_{i,if}^{j} = \frac{g_2^2}{g_2^2 - 1}\hat{N}_{i,1}^{j} - \frac{g_2}{g_2^2 - 1}\hat{N}_{i,2}^{j} \rightarrow \hat{N}_{i,1}^{j} = \frac{g_2 + 1}{g_2}\hat{N}_{i,if}^{j} - \frac{1}{g_2 - 1}\hat{N}_{i,w}^{j} \tag{9}$$

$$\hat{N}_{i,w}^{jk} = \breve{N}_{i,w}^{jk} - \hat{b}_{w}^{jk}; \qquad \hat{N}_{i,1}^{jk} = \frac{g_2 + 1}{g_2}\hat{N}_{i,if}^{jk} - \frac{1}{g_2 - 1}(\breve{N}_{i,w}^{jk} - \hat{b}_{w}^{jk}) \tag{10}$$

$$\hat{b}_n^{jk} = \left\langle \hat{N}_{i,1}^{jk} \right\rangle \tag{11}$$

As already mentioned, three types of satellite-pair phase bias products were used in the following triple-frequency ambiguity resolution. For convenience, we converted single-difference phase biases to their undifferenced styles by selecting a reference satellite.

2.3. Triple-Frequency Ambiguity Resolution

With the help of precise products such as precise satellite clock and orbit and phase bias products, we are able to implement PPP and get the float ambiguities fixed. In triple-frequency PPP-AR, we need to fix (extra-)wide-lane ambiguities first by Equation (12) and further the narrow-lane ambiguities by Equation (13). The (extra-)wide-lane ambiguities should be fixed simultaneously before we try to fix narrow-lane ambiguities.

Before resolving the ambiguities, the initial undifferenced float ambiguities are required to be mapped onto the single-difference counterparts between satellites to eliminate the receiver phase biases. Then the single-difference ambiguities $\hat{N}_{i,1}^{jk}$, $\hat{N}_{i,2}^{jk}$, and $\hat{N}_{i,3}^{jk}$ are used to form the extra-wide-lane and wide-lane ambiguities according to the two equations of Equation (12). The variance–covariance matrix for the raw ambiguities is converted as well to match the combined ambiguities [20]. Once the new matrix is formed, we should inject the extra-wide-lane and wide-lane ambiguities into the Least-squares Ambiguity Decorrelation Adjustment (LAMBDA) function [21] simultaneously to search for their integer candidates. In general, the (extra-)wide-lane ambiguities can be resolved instantaneously and simultaneously [22]. Once these two ambiguities are fixed successfully, other parameters and the corresponding variance–covariance matrix will be updated. The methods for recovering the integer nature of narrow-lane ambiguity are the same as fixing (extra-)wide-lane ambiguities.

$$\begin{cases} \breve{N}_{i,\mathrm{ew}}^{jk} = \hat{N}_{i,2}^{jk} - \hat{N}_{i,3}^{jk} + \hat{b}_{\mathrm{ew}}^{jk} \\ \breve{N}_{i,\mathrm{w}}^{jk} = \hat{N}_{i,1}^{jk} - \hat{N}_{i,2}^{jk} + \hat{b}_{\mathrm{w}}^{jk} \end{cases} \tag{12}$$

$$\breve{N}_{i,1}^{jk} = \frac{g_2}{g_2 - 1}\hat{N}_{i,1}^{jk} - \frac{1}{g_2 - 1}\hat{N}_{i,2}^{jk} - \frac{1}{g_2 - 1}(\breve{N}_{i,w}^{jk} - \hat{b}_w^{jk}) + \hat{b}_n^{jk} \tag{13}$$

It has been mentioned that Geng and Bock (2013) formed an ionosphere-free wide-lane combination with two unambiguous wide-lane ambiguities to improve the rapidity of subsequent narrow-lane ambiguity resolution [13]. The method in this study is equivalent to that of Geng and Bock (2013). In this work, we neither constituted these two wide-lane observables nor form the ionosphere-free wide-lane observables explicitly; rather, we converted the uncombined ambiguities together with their variance–covariance matrix into their extra-wide-lane and wide-lane counterparts for ambiguity resolution. After solving wide-lane ambiguities, the unambiguous ionosphere-free wide-lane observables $L_{i,ifw}^{j}$ are formed implicitly.

$$L_{i,ifw}^{j} = \frac{g_2 g_3}{(g_2 - 1)(g_3 - 1)}L_{i,1}^{j} - \frac{g_3}{(g_2 - 1)(g_3 - g_2)}L_{i,2}^{j} + \frac{g_2}{(g_3 - 1)(g_3 - g_2)}L_{i,3}^{j} \tag{14}$$

Geng et al. (2013) analyzed the noise of the combination observables (noted as amplification factor δ_{noi}). δ_{noi} denotes the phase noise amplification factor of each wide-lane observable [13]. They stated that, although carrier phase noise had been amplified, the unambiguous ionosphere-free wide-lane combination observation was usually more precise than the raw pseudo-range observation. Therefore, we can also study the noise amplification factors of different triple-frequency combinations to analyze the ease of ambiguity resolution. Here we give the noise amplification factors of all possible signal combinations in Table 1. Three typical and suitable signal combinations (E1/E5a/E5b, E1/E5a/E6, and E1/E5/E6) were selected for further analysis. E1/E5a/E5b signals are accepted by most of the multi-frequency receivers. The E1/E5a/E6 signal combination has the lowest noise amplification factor

67.027 [23]. The E1/E5/E6 signal combination is also selected on account of the lower noise and higher multipath anti-interference ability of E5 signals [24]. According to the noise amplification factors, the E1/E5a/E6 combination may obtain the best performance. Further demonstrations and discussions are provided in the following sections.

Table 1. Scaling coefficients of L1, L2, and L3 for ionosphere-free wide-lane observables and the phase noise amplification factors of different Galileo triple-frequency combinations relative to the raw phase observations.

Galileo Signals	L1	L2	L3	δ_{noi}
E1/E5a/E5b	16.892	113.034	−128.926	172.290
E1/E5a/E6	20.969	33.910	−53.879	67.027
E1/E5a/E5	16.216	226.068	−241.284	331.041
E1/E5b/E6	22.716	55.254	−76.970	97.435
E1/E5b/E5	17.567	−257.852	241.284	353.574
E1/E5/E6	21.808	42.580	−63.387	79.414
E5a/E5b/E5	2938.889	3094.222	−6032.111	7389.022
E5a/E5b/E6	440.833	−663.048	223.214	826.916
E5a/E5/E6	881.667	−1064.490	183.824	1394.370
E5b/E5/E6	−1326.095	1064.490	262.605	1720.648

Figure 1 shows the flowchart of triple-frequency PPP-AR process. It combines the main methods described above. The precise satellite clock and phase biases products were calculated at the server end. As for the user end, there are mainly three procedures in the PPP-AR data processing. We carried out PPP and derived float positions and uncombined float ambiguities. Next, the target ambiguities (extra-wide-lane ambiguity, wide-lane ambiguity, and narrow-lane) were computed using the mapping function. Then, using the phase bias corrections and LAMBDA function, we resolved the (extra-)wide-lane ambiguities first and next resolved the narrow-lane ambiguity. Finally, we obtained the results of the triple-frequency PPP-AR.

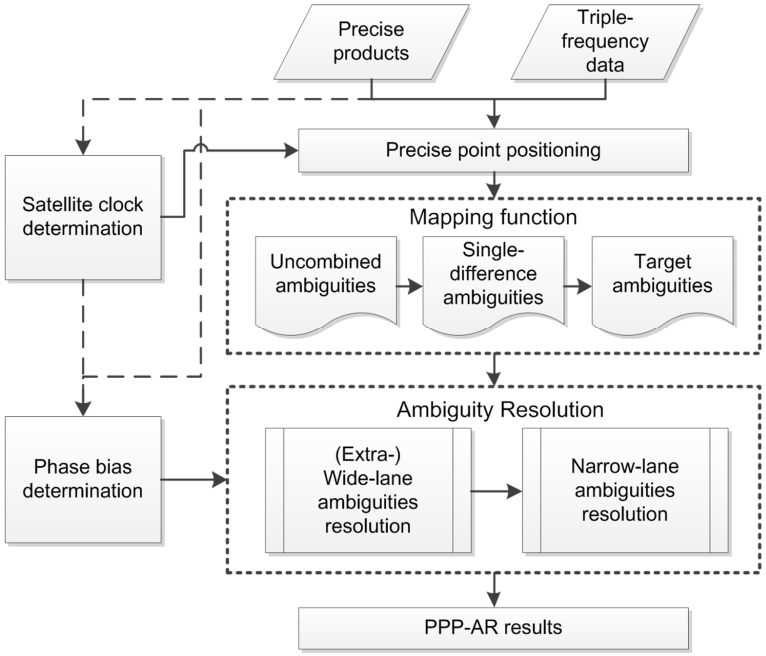

Figure 1. Flowchart of triple-frequency precise point positioning ambiguity resolution (PPP-AR). The satellite clock and phase bias products should be estimated at the server end firstly. Then PPP-AR can be carried out at the user end.

3. Data and Models

The Galileo data used in this study are collected from days 121–150 in 2019. All stations were selected from the IGS Multi-GNSS Experiment (MGEX) and Australian Regional GNSS Network (ARGN). The distribution of all stations is shown in Figure 2. They are all equipped with Septentrio receivers. Fifteen stations were used for Galileo-only kinematic PPP-AR and 21 stations for the estimations of precise Galileo satellite phase biases and clocks. All data were divided into hourly pieces for PPP-AR. The average number of visible Galileo satellites was about seven; note that sessions with less than five satellites were excluded from the analysis. The antenna PCO/PCV corrections were applied for the specific antenna type at each station. Given the lack of official receiver antenna PCO/PCV corrections for Galileo multi-frequency signals, two correction methods were adopted in the processing for comparison. Firstly, the official GPS phase center corrections were used as a replacement. The corrections of GPS L1 signal were used for Galileo L1 signal (E1). The corrections of GPS L2 signal were used for Galileo E5a, E5b, E6, and E5 signals. The second method uses the pilot IGS antenna file to provide parts of receivers' Galileo multi-frequency PCO/PCV corrections. All selected 15 stations have available corresponding corrections in the pilot IGS antenna file and are therefore adopted. Note that Galileo satellite clocks and phase biases were also re-estimated using the pilot IGS antenna file to keep consistency with the user end.

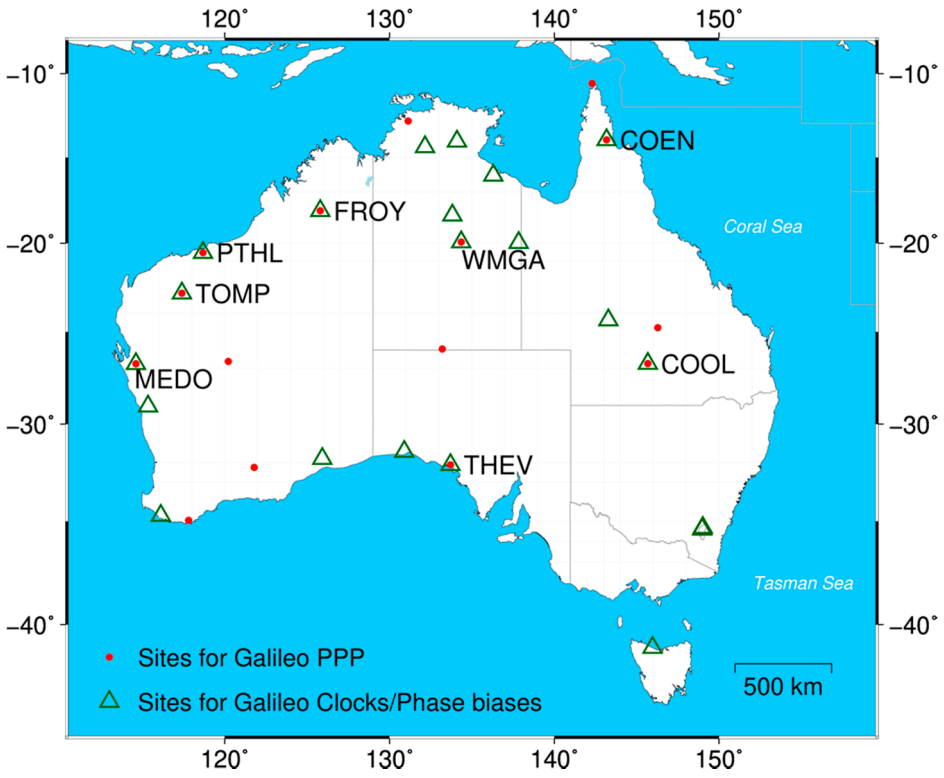

Figure 2. Distribution of stations. There are 15 stations with red dots are used for Galileo kinematic PPP, and 21 stations with dark green triangles are used for the estimations of Galileo satellite phase biases and clocks. The stations used for PPP and product estimation are shown with the site code.

Table 2 shows the data processing strategies in more detail. Both dual- and triple-frequency PPP-AR used the LAMBDA method to search the integer candidates for (extra-)wide-lane and narrow-lane ambiguities. We applied a threshold of 3.0 for the ratio test and adopted the partial ambiguity fixing method [25]. For both dual-frequency and triple-frequency PPP-AR, compared to the known precise station coordinates from daily static PPP solutions, the convergence can be accomplished only if

the positioning errors of the horizontal and vertical components are less than 5 cm and 10 cm for 20 min continuously.

Table 2. Data processing strategies of PPP-AR.

Items	Strategies
Observation	Triple-frequency pseudo-range and carrier phase
Frequency combination	Galileo: E1/E5a, E1/E5a/E5b, E1/E5a/E6, E1/E5/E6
Observation rate	30 s
Cut-off elevation angle	10°
Observation weighting	Elevation-dependent weighting strategy 3 mm and 0.3 m for raw carrier phase and pseudo-range, respectively
Ionosphere delay	Random-walk parameter with a process noise of 0.5 $m/\sqrt{30\ s}$
Troposphere delay	Saastamoinen model [26]; global mapping function (GMF) [27]; estimated hourly with a process noise of 2 $cm/\sqrt{hour}$
PCO/PCV errors	(a) Use an official IGS antenna file (IGS14_2017.atx) to correct the PCO/PCV errors at the satellite end; at the receiver end, use the corrections of GPS for replacement (b) Use a pilot IGS antenna file including all PCO/PCV corrections for Galileo signals at the satellite and receiver ends
Precise products	Use final precise orbit, ERP and multi-GNSS DCB products from CODE; estimate precise satellite clock and phase bias products

4. Results

This section presents the analysis of the characteristics of different Galileo signals and signal combinations for finding the optimum signal combination. It includes a description of the results of PPP-AR with and without using the pilot Galileo receiver antenna phase center corrections to identify if the third-frequency Galileo signals can accelerate precise point positioning ambiguity resolution.

4.1. Characteristics of Different Galileo Signals and Signal Combinations

We used the observations of E1, E5a, E5b, E5, and E6 signals at Station WMGA on day 121, 2019 to study the raw signal qualities. The pseudo-range multipath errors calculated by pseudo-range multipath observable [28] and SNR values of different signals are shown in Figure 3. From the results, we can find that E1, E5a, E5b, and E6 signals have similar SNR values and multipath errors, while E5 signal has significantly higher SNR values and smaller multipath errors. The average multipath errors of E1, E5a, E5b, E5, and E6 signals are −0.0014 m, 0.0011 m, −0.0001 m, 0.0003 m, and 0.0000 m, respectively, and the standard deviations (STDs) are 0.3476 m, 0.2845 m, 0.3107 m, 0.1568 m, and 0.3511 m, respectively. In addition, the average SNR values of E1, E5a, E5b, E5, and E6 signals are 42.1693 dBHz, 42.8437 dBHz, 43.7005 dBHz, 46.2544 dBHz, and 44.2526 dBHz, respectively. The E5 signal shows the best quality, and we verified the phenomenon appears in all days and all stations. However, the raw signal quality is not the only factor affecting the convergence. The noise amplification factors of different triple-frequency combinations require consideration, as they may also affect the convergence of PPP-AR. The amplification factors were introduced in Table 1. That result reveals that the E1/E5a/E6 combination may resolve the ambiguity with the fastest speed considering its relatively small noise. The E1/E5a/E5b combination may be the worst combination of the three selected signal combinations for ambiguity resolution.

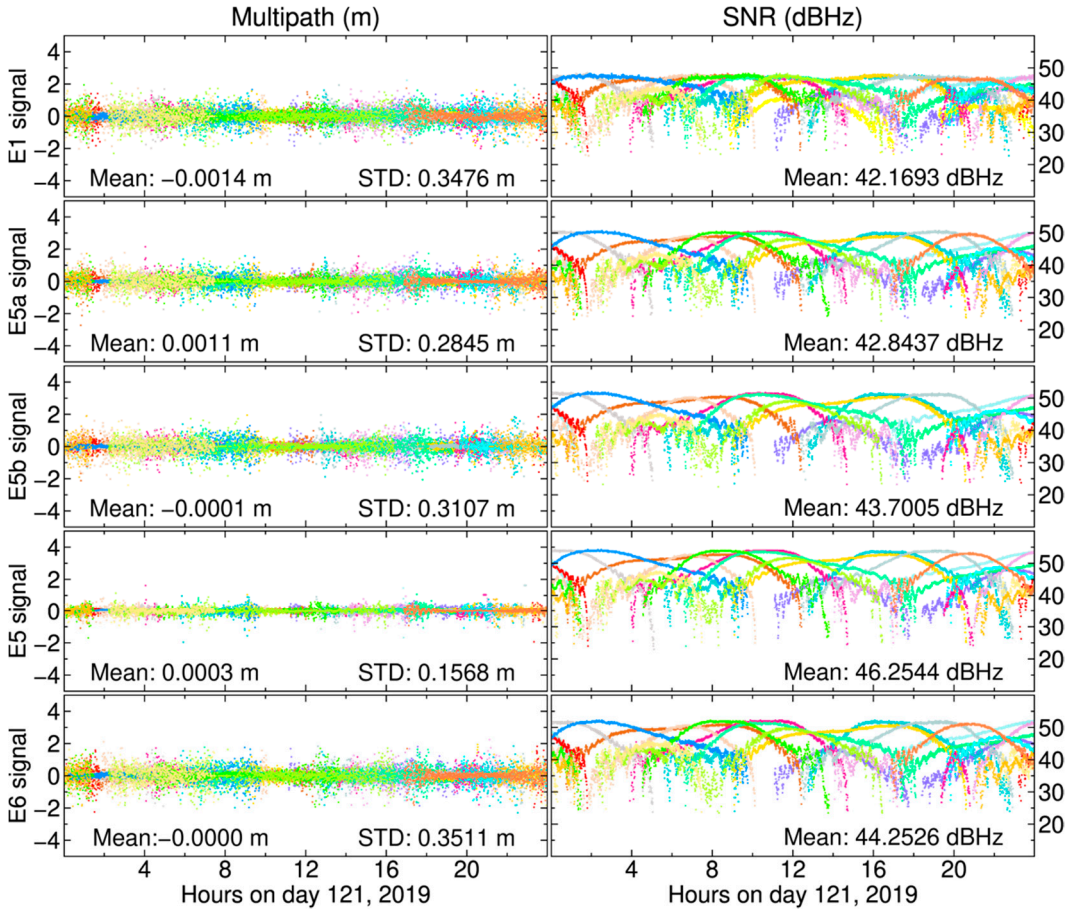

Figure 3. Galileo signal quality analysis for E1, E5a, E5b, E5, and E6. (**left**) The pseudo-range multipath results for all observed Galileo satellites; (**right**) signal-to-noise ratio (SNR) values for all observed Galileo satellites. Different colors denote different Galileo satellites.

4.2. Evaluation of Galileo Phase Biases

The stable and precise phase bias products are necessary for rapid convergence. These were estimated every 15 min during the 30 days of data based on 21 selected stations in this study. Figure 4 shows (extra-)wide-lane and narrow-lane phase biases for all Galileo satellites on day 121, 2019. Subfigures in different rows are for different signal combinations. Different ambiguity resolutions need different phase bias products. The results indicate that the extra-wide-lane phase biases have the best temporal stability due to the long wavelength. The maximum of STDs is under 0.015 cycles for the combination of E1/E5a/E6 and under 0.01 cycles for the E1/E5a/E5b and E1/E5/E6 combinations. The wide-lane phase biases have the secondary temporal stability, and the maximum of STDs is under 0.05 cycles for all used triple-frequency combinations. The temporal stability of the narrow-lane phase biases is not as good as the (extra-)wide-lane phase biases due to the relatively short wavelength, but the maximum of STDs is still under 0.05 cycles. Otherwise, the narrow-lane phase biases generally show a fluctuation at the beginning and become increasingly stable after the convergence. Therefore, no matter which signal combination we use, the calculated Galileo phase biases all have good temporal stability according to the results. Moreover, note that the (extra-)wide-lane phase biases have very good stability throughout the day and can be predicted over a long duration with reliable precision. For the narrow-lane phase biases, the selection of a shorter period is required due to the considerable observed temporal variation. Table 3 shows the mean STDs over the 30 days. The mean STDs of extra-wide-lane, wide-lane, and narrow-lane phase biases for all triple-frequency combinations are under 0.01, 0.015, and 0.02 cycles, respectively. Given the good temporal stabilities, it is likely that Galileo phase biases estimated with different signal combinations can all satisfy the triple-frequency PPP-AR.

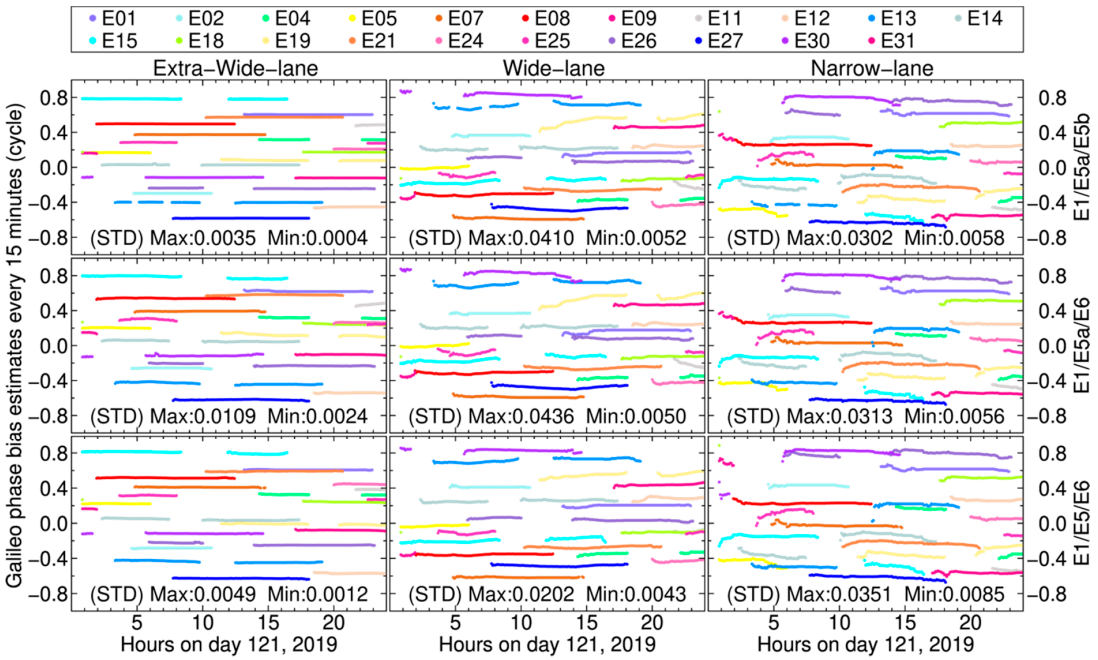

Figure 4. (**left**) Extra-wide-lane, (**middle**) wide-lane, and (**right**) narrow-lane phase biases for all Galileo satellites involved every 15 min on day 121, 2019. The phase biases are estimated based on (**top**) E1/E5a/E5b, (**middle**) E1/E5a/E6, and (**bottom**) E1/E5/E6 signals, respectively. Different colors denote different Galileo satellites. Maximum and minimum of standard deviations (STDs) (**cycle**) of the phase biases of all satellites are shown in each subfigure. Note that the phase biases have been offset vertically to avoid the overlaps. The interrupts in some results are caused by the raw GNSS data.

Table 3. Mean STDs (cycles) of extra-wide-lane, wide-lane and narrow-lane phase biases for all Galileo satellites on all days.

Signals	Extra-Wide-Lane	Wide-Lane	Narrow-Lane
E1/E5a/E5b	0.001	0.013	0.015
E1/E5a/E6	0.005	0.014	0.016
E1/E5/E6	0.006	0.011	0.016

4.3. Results of Triple-Frequency PPP-AR Using the Official GPS Receiver Antenna Corrections

The study of the convergence of Galileo triple-frequency PPP comes down to the narrow-lane ambiguity resolution. Figure 5 shows the positioning errors of a typical station, WMGA. We can see that the narrow-lane ambiguity fixing at the station WMGA is accomplished within 15 min in triple-frequency PPP-AR when using the combination of E1/E5a/E5b. The dual-frequency PPP-AR takes more minutes. The results of E1/E5a/E6 and E1/E5/E6 combinations are worse than the results of dual-frequency PPP-AR. All results of 15 stations in all days were studied. Figure 6 shows the distributions of convergence time for triple-frequency PPP-AR with different triple-frequency combinations (E1/E5a/E5b, E1/E5a/E6, and E1/E5/E6) at 15 stations on all days. When counting the results converged within 5 min, we find that the results of triple-frequency PPP-AR (E1/E5a/E5b, E1/E5a/E6, E1/E5/E6) are all better than the results of dual-frequency PPP-AR. The percentage for the convergence time of dual-frequency PPP-AR within 5 min is only about 8.3%, while the percentages in the case of triple-frequency PPP-AR (E1/E5a/E5b) are about 11.8%. The results using E1/E5a/E6 and E1/E5/E6 combinations are 9.4% and 9.5%, respectively. E1/E5a/E5b processing has the best performance. However, the percentages of successful convergences in less than 20 min for PPP-AR (E1/E5a, E1/E5a/E5b) are more than 45%, whereas the percentages for PPP-AR (E1/E5a/E6 and E1/E5/E6) are less than 40%. The E1/E5a/E6 and E1/E5/E6 combinations even delay the convergence compared with the dual-frequency PPP-AR.

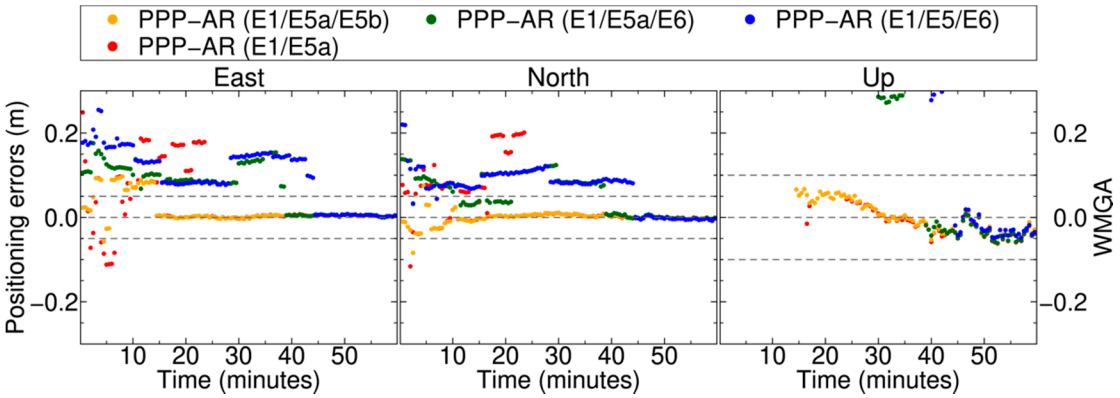

Figure 5. East, north, and up components of 1 h positioning errors (m) at Station WMGA on day 121, 2019. The solutions of dual-frequency (E1/E5a) and triple-frequency (E1/E5a/E5b, E1/E5a/E6, and E1/E5/E6) PPP-AR with the official GPS receiver antenna corrections are shown in different colors. The horizontal dashed lines represent the convergence regions.

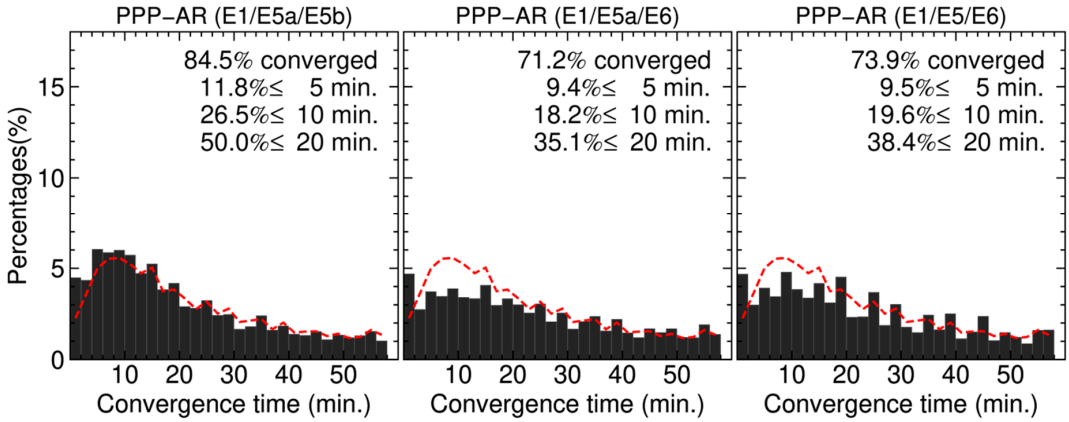

Figure 6. Statistics of the convergence time (minutes) of 15 stations' triple-frequency (E1/E5a/E5b, E1/E5a/E6, and E1/E5/E6) PPP-AR with the official GPS receiver antenna corrections. The percentage of the convergence and the percentages of the convergence time lengths shorter than 5, 10, and 20 min are shown in each subfigure. The red dashed lines represent the percentage distributions of the convergence time of dual-frequency (E1/E5a) PPP-AR.

Furthermore, Table 4 exhibits the mean convergence time for both dual- and triple-frequency PPP-AR in the case of Galileo-only solutions at 15 stations on all days. This table shows 15 stations' results, respectively. We find that most stations' results are improved by using E1/E5a/E5b signals while the results of PPP-AR (E1/E5a/E6, E1/E5/E6) become worse compared with the dual-frequency results. According to the mean results using all stations, PPP-AR (E1/E5a/E5b) reduces the mean convergence time from about 28.9 min to about 26.7 min, i.e., a 7.6% reduction. The STDs of convergence time are also shown in Table 4. All STD values are about 20 min. Note that the number of observed satellites also affects the convergence time deeply. In this study, the average number of observed satellites is about seven. To avoid the situation that lower quality data from a few stations have a deleterious effect on the results as a whole, we tried to remove the stations whose (E1/E5a/E5b, E1/E5a/E6, and E1/E5/E6) triple-frequency PPP-AR all increase by more than 10% compared with the dual-frequency PPP-AR. After removing the three worst stations (ALBY, COOL, NORS), PPP-AR (E1/E5a/E5b) reduced the mean convergence time from about 29.8 min to about 26.2 min, i.e., a 12.1% reduction. However, the results of PPP-AR (E1/E5a/E6, E1/E5/E6) are still unsatisfactory, though the degree of deterioration is reduced from −17.6% and −12.7% to −11.2% and −7.2%.

Table 4. Mean convergence time (minutes) of dual-frequency (E1/E5a) and triple-frequency (E1/E5a/E5b, E1/E5a/E6, and E1/E5/E6) PPP-AR with the official GPS receiver antenna corrections for solutions with respect to each station. The reduction rate of the convergence time of triple-frequency PPP-AR relative to dual-frequency PPP-AR is shown in brackets.

Station Name	PPP-AR E1/E5a	PPP-AR E1/E5a/E5b	PPP-AR E1/E5a/E6	PPP-AR E1/E5/E6
ALBY	25.2	30.6 (−21.5%)	39.3(−56.0%)	36.8 (−45.9%)
COEN	39.5	39.6 (−0.3%)	45.7 (−15.6%)	45.8 (−15.9%)
COOL	26.1	30.6 (−17.3%)	39.4 (−50.8%)	38.2 (−46.1%)
DARW	46.4	39.8 (14.2%)	45.2 (2.6%)	44.1 (5.1%)
FROY	28.9	23.2 (19.8%)	29.1 (−0.6%)	28.7 (0.6%)
HNIS	30.7	30.2 (1.6%)	36.2 (−18.0%)	35.1 (−14.3%)
MEDO	29.2	25.9 (11.2%)	31.3 (−7.1%)	30.4 (−4.2%)
MTCV	21.9	18.2 (16.8%)	27.9 (−27.4%)	26.0 (−18.6%)
NORS	22.6	27.5 (−21.3%)	37.0 (−63.2%)	34.3 (−51.5%)
PTHL	23.4	20.5 (12.4%)	26.8 (−14.4%)	26.0 (−11.1%)
THEV	25.2	21.7 (14.1%)	31.3 (−24.3%)	29.4 (−16.5%)
TMBO	40.1	32.8 (18.3%)	39.9 (0.7%)	38.0 (5.2%)
TOMP	25.9	23.6 (8.7%)	29.3 (−13.2%)	27.6 (−6.5%)
WILU	23.2	20.5 (11.6%)	30.3 (−30.6%)	29.3 (−26.2%)
WMGA	26.2	20.6 (21.6%)	28.8 (−9.8%)	28.5 (−8.6%)
Mean (15 stations)	28.9	26.7 (7.6%)	34.0 (−17.6%)	32.6 (−12.7%)
STD (15 stations)	19.9	19.9	21.3	21.1
Mean (12 stations)	29.8	26.2 (12.1%)	33.1 (−11.2%)	31.9 (−7.2%)
STD (12 stations)	19.9	19.7	21.3	21.0

4.4. Results of triple-frequency PPP-AR using the pilot Galileo receiver antenna corrections

When applying the new pilot receiver antenna PCO/PCV corrections for Galileo multi-frequency signals, the positioning errors of station WMGA are shown in Figure 7 for comparison. Both E1/E5a/E6 and E1/E5/E6 PPP-AR achieve convergence within 15 min, and these results are a little bit better than the results of E1/E5a/E5b PPP-AR. The distributions of convergence time for triple-frequency PPP-AR (E1/E5a/E5b, E1/E5a/E6 and E1/E5/E6) at 15 stations on all days are shown in Figure 8. When examining the results converged within 5 min, we find that the results of triple-frequency PPP-AR (E1/E5a/E5b, E1/E5a/E6, E1/E5/E6) are all better than the results of dual-frequency PPP-AR. The similar bad phenomenon described in Section 4.3 does not appear in the results using the pilot Galileo receiver antenna PCO/PCV corrections. The percentage for the convergence time of dual-frequency PPP-AR within 5 min is only about 8.2% while the percentages in the case of triple-frequency PPP-AR (E1/E5a/E5b, E1/E5a/E6, and E1/E5/E6) are about 12.5%, 21.6%, and 16.5%, respectively. Overall, the E1/E5a/E6 processing has the best performance, and all three types of triple-frequency PPP-AR can achieve convergence in a shorter time compared with dual-frequency PPP-AR.

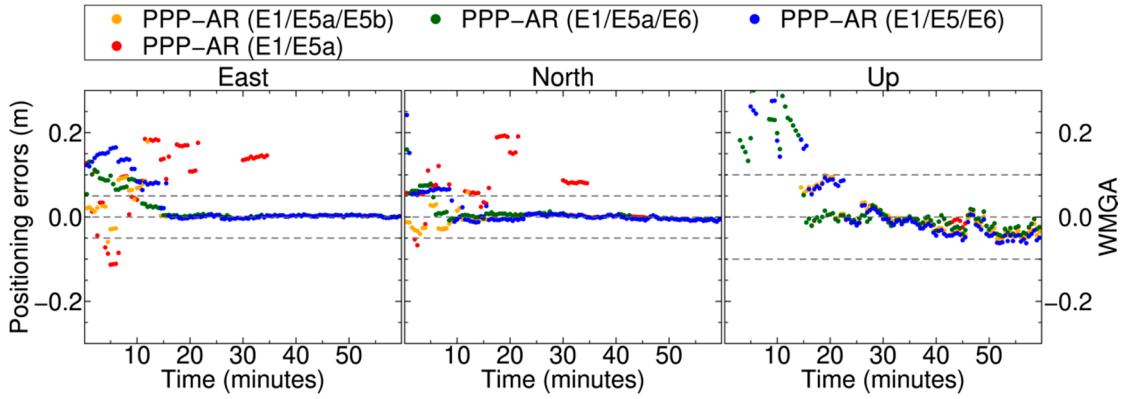

Figure 7. East, north, and up components of 1 h positioning errors (m) at Station WMGA on day 121, 2019. The solutions of dual-frequency (E1/E5a) and triple-frequency (E1/E5a/E5b, E1/E5a/E6, and E1/E5/E6) PPP-AR with the pilot Galileo receiver antenna corrections are shown in different colors. The horizontal dashed lines represent the convergence regions.

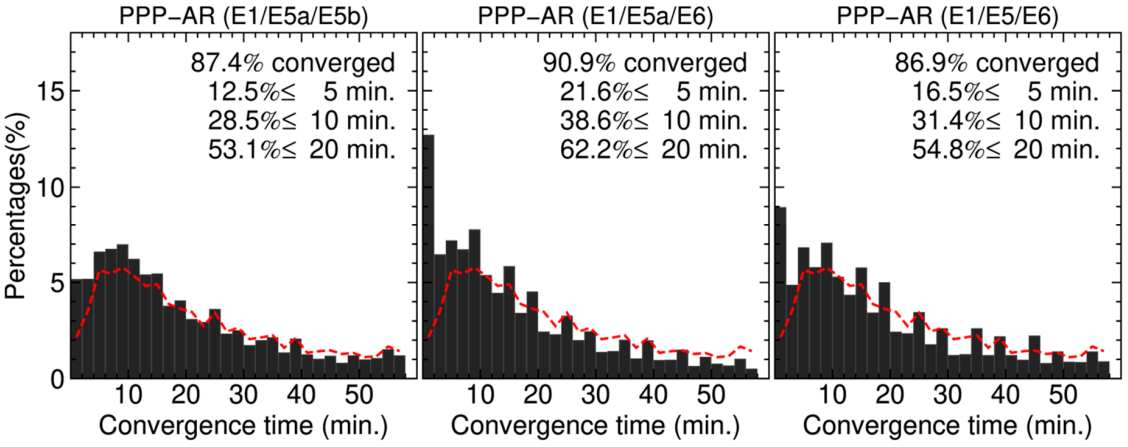

Figure 8. Statistics of the convergence time (minutes) of 15 selected stations' triple-frequency (E1/E5a/E5b, E1/E5a/E6, and E1/E5/E6) PPP-AR with the pilot Galileo receiver antenna corrections. The percentage of the convergence and the percentages of the convergence time lengths shorter than 5, 10, and 20 min are shown in each subfigure. The red dashed lines represent the percentage distributions of the convergence time of dual-frequency (E1/E5a) PPP-AR.

Table 5 exhibits the mean convergence time for both dual- and triple-frequency PPP-AR with the pilot PCO/PCV corrections at 15 stations on all days. When we used the pilot receiver antenna PCO/PCV corrections that include the corrections for Galileo multi-frequency signals, all types of PPP-AR could yield better results. In addition, triple-frequency PPP-AR based on E1/E5a/E5b, E1/E5a/E6, and E1/E5/E6 signals speeds up the convergence on average by about 16.2%, 30.3%, and 17.7%, respectively. In addition, all STDs for the results of triple-frequency PPP-AR are reduced compared with the results in Section 4.3, and the convergence time of E1/E5a/E6 PPP-AR has the smallest STD value equal to 18.2 min. The superiority of E1/E5a/E6 signals is apparent. Therefore, the receiver antenna PCO/PCV errors were probably mitigated by the pilot Galileo antenna phase center corrections. Comparing the results with and without using the pilot antenna corrections, it is likely that the receiver PCO/PCV errors affect the convergence of PPP-AR significantly, and they deserve more attention. The results in this section demonstrate the reliability of the performances of different triple-frequency PPP-AR. The signal combination E1/E5a/E6 is shown to have the smallest noise amplification factor. According to the results of PPP-AR, the combination of E1/E5a/E6 is recommended for use in preference to others.

Table 5. Mean convergence time (min) of dual-frequency (E1/E5a) and triple-frequency (E1/E5a/E5b, E1/E5a/E6, and E1/E5/E6) PPP-AR with the pilot Galileo receiver antenna corrections for solutions with respect to each station. The reduction rate of the convergence time of triple-frequency PPP-AR relative to dual-frequency PPP-AR is shown in brackets.

Station Name	PPP-AR E1/E5a	PPP-AR E1/E5a/E5b	PPP-AR E1/E5a/E6	PPP-AR E1/E5/E6
ALBY	24.5	21.6 (11.6%)	19.4 (20.8%)	24.2 (1.3%)
COEN	39.3	34.8 (11.4%)	30.5 (22.5%)	33.8 (14.0%)
COOL	25.8	21.8 (15.6%)	18.7 (27.4%)	22.8 (11.9%)
DARW	46.3	38.1 (17.7%)	35.8 (22.7%)	38.2 (17.6%)
FROY	29.1	23.3 (19.7%)	18.6 (36.1%)	21.7 (25.2%)
HNIS	29.8	25.7 (13.8%)	22.3 (25.0%)	27.1 (9.0%)
MEDO	29.2	26.4 (9.5%)	20.2 (30.8%)	23.9 (18.1%)
MTCV	22.5	18.3 (18.3%)	14.7 (34.4%)	17.1 (23.9%)
NORS	21.3	19.2 (10.2%)	14.1 (33.8%)	20.5 (3.9%)
PTHL	23.3	20.3 (12.7%)	17.2 (25.6%)	20.4 (12.5%)
THEV	25.4	20.9 (17.8%)	16.4 (35.3%)	20.0 (21.0%)
TMBO	39.9	25.4 (36.2%)	22.2 (44.3%)	24.7 (38.2%)
TOMP	26.1	24.2 (7.5%)	19.0 (27.1%)	22.9 (12.5%)
WILU	24.0	20.5 (14.7%)	16.4 (31.7%)	20.2 (16.0%)
WMGA	26.0	20.7 (20.7%)	17.1 (34.3%)	20.4 (21.8%)
Mean (15 stations)	28.6	24.0 (16.2%)	19.9 (30.3%)	23.5 (17.7%)
STD (15 stations)	19.9	18.9	18.2	19.5

5. Discussion

Multi-frequency GNSS processing will become more important with the development of GNSS. In this paper, we first showed the difference among the performance of triple-frequency PPP-AR based on different signal combinations. E1/E5a/E5b signals were usually used in previous research, but the contributions of other signal combinations are unclear [14,15,29,30]. We then discuss the receiver antenna phase center errors for Galileo signals. Such errors were usually corrected using the GPS corrections due to the lack of Galileo corrections in the current official IGS antenna file [14,15,29]. Li et al. (2018) also used GPS corrections for BeiDou signals due to the receiver antenna PCO/PCV corrections not being available for BeiDou signals [12].

Geng et al. (2020) indicated that a small part of multi-GNSS triple-frequency PPP-AR results became unexpectedly worse compared to the results of dual-frequency PPP-AR [14]. Cao et al. (2018) also pointed out that some ambiguities were not fixed to integers in their results [15]. The E1/E5a/E5b PPP-AR in this paper using the official IGS antenna file had also worse results than those from E1/E5a PPP-AR. Most results of triple-frequency PPP-AR using E1/E5a/E6 and E1/E5/E6 signals were also not as good as expected. However, after using the pilot IGS antenna file, all results in this paper were improved. Therefore, the receiver antenna phase center errors are not negligible. We do not recommend applying the GPS receiver antenna PCO/PCV corrections to other GNSS satellites in triple-frequency PPP-AR data processing.

The results using E1/E5a/E6 signals were better than those using other signal combinations. E1/E5a/E6 triple-frequency processing could achieve the PPP convergence within 19.9 min on average. Moreover, the phase noise amplification factor given and analyzed in some previous research is worthy of consideration [13,14]. According to the basic analysis of the phase noise amplification factors of different triple-frequency combinations and the corresponding PPP-AR results in this paper, it is likely that the smaller the amplification factor is, the faster the convergence can be. This analysis can aid in finding a better signal combination with smaller noise that could benefit triple-frequency PPP-AR.

6. Conclusions

In this study, we focused on the convergence of Galileo triple-frequency PPP-AR with different triple-frequency combinations (E1/E5a/E5b, E1/E5a/E6, and E1/E5/E6). We analyzed the raw qualities of different signals and the noise amplification factors of different signal combinations. We found that the E5 signal has the smallest multipath and the highest SNR relative to the other signals. E1/E5a/E6 combination has the smallest noise amplification factor, which can benefit the ambiguity resolution and speed up the convergence. According to the results and discussion, the noise amplification factor plays an important role in the convergence for the triple-frequency PPP-AR method adopted in this paper.

We implemented triple-frequency PPP-AR using precise satellite phase biases. The means of STDs of extra-wide-lane, wide-lane, and narrow-lane phase biases were lower than 0.01, 0.015, and 0.02 cycles, respectively. The results of phase biases had good stability enabling us to realize ambiguity resolution. According to the results of PPP-AR for the 15 stations using the official GPS receiver antenna corrections, for PPP-AR, only the results of using the combination (E1/E5a/E5b) showed marginal improvement relative to dual-frequency PPP-AR. The results of the other two triple-frequency combinations were even worse than the results of dual-frequency PPP-AR. By carrying out further experiments with the pilot Galileo receiver antenna corrections, we found that the advantages of triple-frequency combinations are negated by the receiver antenna phase center errors.

After adopting the pilot IGS antenna file, we compared the results with and without using the new pilot receiver antenna PCO/PCV corrections for Galileo multi-frequency signals. In detail, PPP-AR with the E1/E5a/E6 combination could acquire the best positioning performance, and the convergences could be realized within an average of 19.9 min. Triple-frequency PPP-AR with the E1/E5a/E5b combination had a longer mean convergence time of 24 min. Triple-frequency PPP-AR with the E1/E5/E6 combination had a moderate convergence time of 23.5 min, and dual-frequency PPP-AR even needed 28.6 min for the convergence. Triple-frequency PPP-AR based on E1/E5a/E5b, E1/E5a/E6, and E1/E5/E6 signals speeded up the convergence on average by about 16.2%, 30.3%, and 17.7%, respectively. In addition, 21.6% results of PPP-AR with the E1/E5a/E6 combination could be converged within 5 min, while the percentage for the E1/E5a/E5b combination was only 12.5%. The results of PPP-AR (E1/E5a/E6) were encouraging and attractive.

The results using the pilot Galileo receiver antenna corrections indicate how each of the candidate third-frequency signals contributes to fast PPP-AR reliability. The receiver antenna PCO/PCV errors in multi-frequency processing are probably underrated, and the GPS receiver antenna PCO/PCV corrections are not recommended for different GNSS satellite signals.

In summary, using Galileo triple-frequency signals can enhance the performance of PPP-AR. The triple-frequency signal combination E1/E5a/E6 is more efficient in achieving rapid PPP-AR, and the E1/E5a/E6 combination is preferred. Considering the impact of the receiver antenna PCO/PCV corrections is not negligible, the development of the Galileo system and the release of the authoritative complete PCO/PCV products in the future can further speed up the convergence of multi-frequency PPP-AR.

Author Contributions: Conceptualization, J.G. (Jianghui Geng); Methodology, J.G. (Jiang Guo); Software, J.G. (Jiang Guo); Validation, S.X. and J.G. (Jiang Guo); Formal analysis, S.X.; Investigation, J.G. (Jiang Guo); Data curation, J.G. (Jiang Guo); Writing—original draft preparation, S.X.; Writing—review and editing, J.G. (Jianghui Geng) and X.M.; Visualization, S.X.; Supervision, J.G. (Jianghui Geng). All authors have read and agreed to the published version of the manuscript.

Funding: This study was funded by National Natural Science Foundation of China (41674033) and National Key Research and Development Program of China (2018YFC1503601). This study was supported by "the Fundamental Research Funds for the Central Universities".

Acknowledgments: We thank IGS (International GNSS Service) and ARGN (Australian Regional GNSS Network) for the multi-GNSS data and the high-quality satellite products. We are grateful to Arturo Villiger for his provision of the pilot Galileo antenna corrections (arturo.villiger@aiub.unibe.ch). The computation work was done on the high-performance computing facility of Wuhan University. Simon Roberts at the University of Nottingham in the UK has proofread this manuscript.

Conflicts of Interest: The authors declare no conflict of interest.

References

1. Odolinski, R.; Teunissen, P.J.G.; Odijk, D. Combined BDS, Galileo, QZSS and GPS single-frequency RTK. *GPS Solut.* **2015**, *19*, 151–163. [CrossRef]
2. Teunissen, P.J.G.; Odolinski, R.; Odijk, D. Instantaneous BeiDou + GPS RTK positioning with high cut-off elevation angles. *J. Geod.* **2014**, *88*, 335–350. [CrossRef]
3. Zumberge, J.F.; Heflin, M.B.; Jefferson, D.C.; Watkins, M.M.; Webb, F.H. Precise point positioning for the efficient and robust analysis of GPS data from large networks. *J. Geophys. Res.* **1997**, *102*, 5005–5017. [CrossRef]
4. Liu, Y.; Lou, Y.; Ye, S.; Zhang, R.; Song, W.; Zhang, X.; Li, Q. Assessment of PPP integer ambiguity resolution using GPS, GLONASS and BeiDou (IGSO, MEO) constellations. *GPS Solut.* **2017**, *21*, 1647–1659. [CrossRef]
5. Geng, J.; Guo, J.; Chang, H.; Li, X. Toward global instantaneous decimeter-level positioning using tightly coupled multi-constellation and multi-frequency GNSS. *J. Geod.* **2019**, *93*, 977–991. [CrossRef]
6. Wübbena, G.; Schmitz, M.; Bagge, A. PPP-RTK: Precise point positioning using state-space representation in RTK networks. In Proceedings of the ION GNSS 2005 18th International Technical Meeting of the Satellite Division, Long Beach, CA, USA, 13–16 September 2005; pp. 2584–2594.
7. Geng, J.; Meng, X.; Dodson, A.H.; Ge, M.; Teferle, F.N. Rapid re-convergences to ambiguity-fixed solutions in precise point positioning. *J. Geod.* **2010**, *84*, 705–714. [CrossRef]
8. Geng, J.; Shi, C. Rapid initialization of real-time PPP by resolving undifferenced GPS and GLONASS ambiguities simultaneously. *J. Geod.* **2017**, *91*, 361–374. [CrossRef]
9. Feng, Y. GNSS three carrier ambiguity resolution using ionosphere-reduced virtual signals. *J. Geod.* **2008**, *82*, 847–862. [CrossRef]
10. Vollath, U.; Birnbach, S.; Landau, L.; Fraile-ordonez, J.M.; Marti-neira, M. Analysis of three-carrier ambiguity resolution (TCAR) technique for precise relative positioning in GNSS-2. In Proceedings of the 11th International Technical Meeting of the Satellite Division of The Institute of Navigation (ION GPS 1998), Nashville, TN, USA, 15–18 September 1998; pp. 417–426.
11. Hatch, R. A new three-frequency, geometry-free technique for ambiguity resolution. In Proceedings of the ION GNSS 2006, Fort Worth, TX, USA, 26–29 September 2006; pp. 309–316.
12. Li, P.; Zhang, X.; Ge, M.; Schuh, H. Three-frequency BDS precise point positioning ambiguity resolution based on raw observables. *J. Geod.* **2018**. [CrossRef]
13. Geng, J.; Bock, Y. Triple-frequency GPS precise point positioning with rapid ambiguity resolution. *J. Geod.* **2013**, *87*, 449–460. [CrossRef]
14. Geng, J.; Guo, J.; Meng, X.; Gao, K. Speeding up PPP ambiguity resolution using triple-frequency GPS/BeiDou/Galileo/QZSS data. *J. Geod.* **2020**. [CrossRef]
15. Cao, X.; Li, J.; Zhang, S.; Kuang, K.; Gao, K.; Zhao, Q.; Hong, H. Uncombined precise point positioning with triple-frequency GNSS signals. *Adv. Space Res.* **2018**. [CrossRef]
16. Odijk, D.; Zhang, B.; Khodabandeh, A.; Odolinski, R.; Teunissen, P.J.G. On the estimability of parameters in undifferenced, uncombined GNSS network and PPP-RTK user models by means of S-system theory. *J. Geod.* **2016**, *90*, 15–44. [CrossRef]
17. Zhang, B.; Teunissen, P.J.G.; Odijk, D.; Ou, J.; Jiang, Z. Rapid integer ambiguity-fixing in precise point positioning. *Chin. J. Geophys.* **2012**, *55*, 2203–2211. (In Chinese)
18. Guo, J.; Geng, J. GPS satellite clock determination in case of inter-frequency clock biases for triple-frequency precise point positioning. *J. Geod.* **2018**, *92*, 1133–1142. [CrossRef]
19. Ge, M.; Gendt, G.; Rothacher, M.; Shi, C.; Liu, J. Resolution of GPS carrier-phase ambiguities in precise point positioning (PPP) with daily observations. *J. Geod.* **2008**, *82*, 389–399. [CrossRef]
20. Dong, D.; Bock, Y. Global positioning system network analysis with phase ambiguity resolution applied to crustal deformation studies in California. *J. Geophys. Res.* **1989**, *94*, 3949–3966. [CrossRef]
21. Teunissen, P.J.G. The least-squares ambiguity decorrelation adjustment: A method for fast GPS integer ambiguity estimation. *J. Geod.* **1995**, *70*, 65–82. [CrossRef]
22. Teunissen, P.J.G.; Joosten, P.; Tiberius, C. A comparison of TCAR, CIR and LAMBDA GNSS ambiguity resolution. In Proceedings of the ION GPS 2002, Portland, OR, USA, 24–27 September 2002; pp. 2799–2808.

23. Geng, J.; Guo, J. Beyond three frequencies: An extendable model for single-epoch decimeter-level point positioning by exploiting Galileo and BeiDou-3 signals. *J. Geod.* **2020**, *94*. [CrossRef]
24. Zaminpardaz, S.; Teunissen, P.J.G. Analysis of Galileo IOV + FOC signals and E5 RTK performance. *GPS Solut.* **2017**, *21*, 1855–1870. [CrossRef]
25. Saastamoinen, J. Contribution to the theory of atmospheric refraction: Refraction corrections in satellite geodesy. *Bull. Geod.* **1973**, *107*, 13–34. [CrossRef]
26. Boehm, J.; Niell, A.E.; Tregoning, P.; Schuh, H. The Global Mapping Function (GMF): A new empirical mapping function based on data from numerical weather model data. *Geophys. Res. Lett.* **2006**, *33*, L07304. [CrossRef]
27. Teunissen, P.J.G. An optimality property of the integer least-squares estimator. *J. Geod.* **1999**, *73*, 587–593. [CrossRef]
28. Seepersad, G.; Bisnath, S. Reduction of PPP convergence period through pseudorange multipath and noise mitigation. *GPS Solut.* **2014**, *19*, 369–379. [CrossRef]
29. Wang, K.; Khodabandeh, A.; Teunissen, P.J.G. Five-frequency Galileo long-baseline ambiguity resolution with multipath mitigation. *GPS Solut.* **2018**, *22*. [CrossRef]
30. Tu, R.; Liu, J.; Zhang, R.; Zhang, P.; Huang, X.; Lu, X. RTK model and positioning performance analysis using Galileo four-frequency observations. *Adv. Space Res.* **2019**, *63*, 913–926. [CrossRef]